https://doi.org/10.1051/epjconf202328901001
EPJ Web of Conferences **289**, 01001 (2023)
FCCP2022
FERMILAB-CONF-23-0887-V

Status of the Muon $g-2$ experiment

Peter Winter[1,*]

[1]*Argonne National Laboratory, Lemont, IL 60439, USA*

Abstract. The Muon $g-2$ Experiment at Fermi National Accelerator Laboratory was designed to measure the anomalous magnetic moment of the muon, a_μ, with a precision of 140 parts-per-billion; a four-fold improvement over the former BNL measurement. The Fermilab experiment was motivated by the about 3.5 standard deviation between the experiment and the Standard Model calculation of a_μ which could be a hint of new physics. The experiment at Fermilab relies on the well-established storage ring technique using magic momentum muons but employs new detector systems and a higher rate of muons per injection cycle to achieve the significant improvement in precision. A first result from the Run-1 data taking period has achieved an uncertainty of 0.46 parts-per-million and confirmed the BNL discrepancy, further increasing the tension with the Standard Model to $4.2\,\sigma$. The experimental technique, key aspects of the measurement, and the data analysis of Run-1 will be summarized.

1 Introduction

The magnetic moment $\vec{\mu}$ of a charged elementary particle is linked to its spin $\vec{S}$ via the gyro-magnetic ratio g. For the structure-less, spin-$\frac{1}{2}$ electron, the Dirac equation predicted $g_e \equiv 2$ [1] while virtual particle loops give rise to small additional contributions known as the anomalous magnetic moment, $a_\mu = \frac{1}{2}(g_\mu - 2)$. The dominant contribution, the so-called Schwinger term, is of size $\alpha/2\pi$ [2] and arises from the coupling of a virtual photon to the muon.

The understanding of the anomalous magnetic moments of electrons and muons have played an essential role in the formulation of our current understanding of fundamental particles and their interactions, the so-called Standard Model (SM) of Particle Physics. The measurement of the electron's anomalous magnetic moment [3] offers one of the most precise determinations of the fine structure constant, α_{QED} or in conjunction with other measurements of α [4, 5] the most precise test of QED. The muon anomalous magnetic moment, a_μ, is more sensitive to contributions from heavier particles by a factor of $(m_\mu^2/m_e^2) \approx 42000$ compared to the electron. As many extensions to the SM predict heavy new particles, a correct prediction of a_μ is an important test for any new theory.

On the experimental side, there has been a long-standing history of continual improvements in the precision of a_μ. The latest milestone prior to the E989 Muon g–2 experiment at Fermilab was reached by the Brookhaven E821 experiment [6]. The about $3.5\,\sigma$ deviation between the experiment and the SM calculation was a possible hint of new physics and motivated the new Muon $g-2$ experiment at Fermilab, which was designed with a precision goal of 140 part-per-billion (ppb) [7]. Assuming that the central values of both SM and experiment remained the same this improved precision would lead to $5\,\sigma$ signal of new physics. The first result [8–11] from the new experiment is based on the analysis of the Run-1 data. The result confirmed the BNL measurement with similar precision. The difference of the experimental world average of $(116,592,061 \pm 41) \times 10^{-11}$ (350 ppb) with the current SM [12–32] is $(251 \pm 59) \times 10^{-11}$ or $4.2\,\sigma$ as shown in Fig. 1.

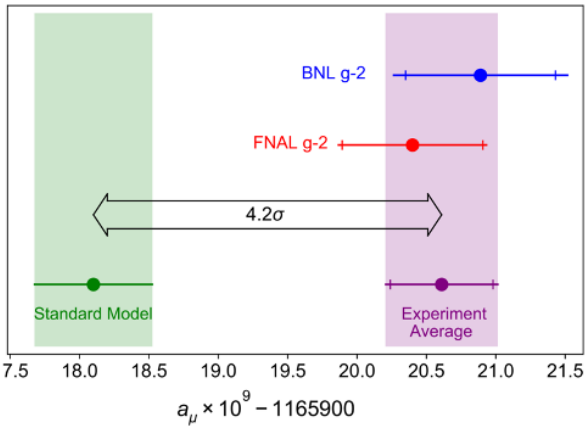

Figure 1. Run-1 result for a_μ from the Fermilab experiment together with the former BNL result [6], the new weighted experimental average, and the SM value [12].

The SM calculation for the anomalous magnetic moment, a_μ, includes electromagnetic, weak, and strong corrections The largest theoretical uncertainty stems from the first-order hadronic vacuum polarization (HVP), which is evaluated from low energy e^+e^- data via a dispersion relation. Significant improvement in the precision in re-

*e-mail: winterp@anl.gov

cent years came from new, precise data from the CMD and SND experiments at Novosibirsk, KLOE at Frascati, BaBar at SLAC, and Belle at KEK. A recent result from CMD-3 [33] for the two pion channel shows a significant discrepancy to other experimental measurements in this low-energy regime and will require further investigations.

In past years, lattice-QCD has also made significant progress but results using this approach were not as precise as the dispersive approach and hence not yet used in the current SM value for the HVP [12]. However, a lattice-QCD result by the BMW collaboration with sub-percent precision [34] was released in 2021 and showed tension with the HVP value obtained from the data-driven approach using the dispersion relation. Recently, the lattice-QCD community focused on the so-called intermediate window energy range which reduces the dominant systematic uncertainties entering the full HVP determination. Results for the determination of a_μ in the intermediate window [34–41] show confirmation of the BMW value and further effort is needed to understand the discrepancy between lattice-QCD and data-driven determinations of the HVP. More details on the theoretical work for a_μ are presented in other contributions to these proceedings.

2 The Fermilab Muon $g-2$ experiment

The Fermilab Muon $g-2$ experiment is based on the storage ring technique established at CERN [42–44] and BNL [6]. To reach the fourfold improvement in precision on a_μ, many of the detection systems used at BNL were replaced or significantly upgraded.

2.1 Muon production, injection, and storage

The muons are produced at Fermilab via proton collisions in the former anti-proton production target. Positive pions produced in the target are momentum selected and decay into muons in the transport beam line to the experimental hall. Due to parity violation of the weak force, the resulting, highly polarized muon beam is injected into the superconducting 1.45 T storage ring shown in Fig. 2, which was relocated from Brookhaven.

The muons enter the storage ring through an inflector magnet [45]. The inflector is a non-ferrous, double cosine theta, superconducting magnet that's placed inside the main magnet yoke to cancel the storage B-field. The resulting field-free channel offers the muons a path to enter the storage area of the main magnet. Since they are displaced radially outwards by 77 mm from the ideal orbit, the muons would be lost during their first turn. A set of 3 new, fast kicker magnets [46] were built to deflect the muons after a quarter turn onto the ideal orbit. The system uses a Blumlein design to deliver the fast kicking pulse with a pulse length of less than 149 ns, the revolution time of the muons in the storage ring. Pulsed, electric quadrupoles [47] are employed to contain the muons vertically.

The relevant observable for the anomalous precession frequency, ω_a, is the rate of change of $\hat{\beta}\cdot\vec{S}$, where $\hat{\beta}$ and $\vec{S}$ are the directions of the muon's momentum and spin, respectively. Since the angle between the muon's spin precession, $\vec{\omega}_s$, and its cyclotron precession, $\vec{\omega}_c$, is small, the rate change of $\hat{\beta}\cdot\vec{S}$ can be approximated by $\vec{\omega}_a$, which in the presence of the magnetic, $\vec{B}$, and electric field, $\vec{E}$, is:

$$\vec{\omega}_a \equiv \vec{\omega}_s - \vec{\omega}_c = -\frac{q}{m}\left[a_\mu\vec{B} - \left(a_\mu - \frac{1}{\gamma^2-1}\right)\frac{\vec{\beta}\times\vec{E}}{c} - a_\mu\left(\frac{\gamma}{\gamma+1}(\vec{\beta}\cdot\vec{B})\vec{\beta}\right)\right] \quad (1)$$

For horizontally circulating muons in a vertical magnetic field, $\vec{\beta}\cdot\vec{B}=0$, rendering the term in the second line zero. This condition is approximately met in the Muon g-2 experiment. To overcome the term from the motional magnetic field induced by the electric field, $\vec{\beta}\times\vec{E}/c$, the CERN-III, BNL, and Fermilab experiments use muons at the "magic" momentum ($\gamma = 29.3$, $p = 3.096\,\mathrm{GeV}/c$), where $a_\mu - 1/(\gamma^2-1) = 0$. A future $g-2$/EDM experiment at J-PARC [48] takes a different approach using weak magnetic focusing, e.g. $\vec{E}=0$. With these conditions met, Eq. (1) simplifies Eq. (1) to

$$\omega_a = \frac{e}{m}a_\mu|\vec{B}|, \quad (2)$$

showing that the determination of a_μ requires precise measurements of the anomalous spin precession frequency of the muons, ω_a, and the magnetic field, $\vec{B}$. Corrections due to vertical motion of the muons (pitch correction) and the off-magic momentum distribution (E-field correction) will be discussed in Sec. 3.

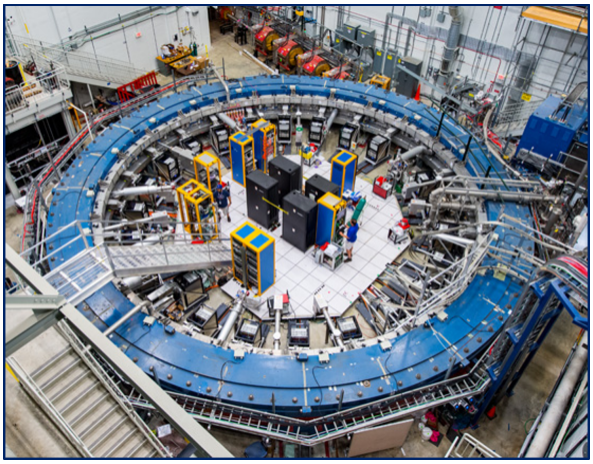

Figure 2. An image of the storage ring during the Run-1 data taking period. Credit: Reidar Hahn, Fermilab.

2.2 Muon anomalous precession and magnetic field measurements

The muons mainly decay via $\mu \to e\nu\bar{\nu}$ with a time-dilated lifetime of $\tau \approx 64\,\mu\mathrm{s}$. Due to the parity violating weak decay, the positrons' direction carries an energy-dependent asymmetry A(E) with respect to the muon's spin. The experiment is equipped with 24 calorimeter stations placed

radially inwards with respect to the muon storage region. Each calorimeter consists of 54 PbF_2 Cherenkov crystals readout with silicon photomultipliers (SiPM) [49–51]. The signals from the SiPMs are digitized in custom-made 800 mega-samples per second digitizers. The calorimeters determine the the energy and time of the decay positrons and the segmentation suppressed systematic effects from pile-up. The measured positron rate in the calorimeters is an exponential modulated by ω_a. A fit to the data allows for the extraction of ω_a as detailed in Sec. 3. The gain of each calorimeter crystal is monitored with a sophisticated laser calibration system [52]. The major gain systematics are the infill gain change of order 10 µs and double pulse gain change of order 10 ns.

The precise measurement of the averaged magnetic field as seen by the stored muon ensemble is achieved by using nuclear magnetic resonance (NMR) of protons in water, a technique pioneered by Bloch [53] and Purcell [54]. The averaged azimuthal field distribution is mapped with an in-vacuum field camera [55], the so-called trolley. It is equipped with 17 NMR probes and provides detailed maps of the magnetic field during periods without stored muons every 3-5 days. 378 fixed NMR probes continuously monitor the field above and below the muon storage aperture during the trolley maps and muon injection. An additional probe with a cylindrical water sample [56] provides the absolute calibration of the magnetic field in terms of the shielded proton Larmor frequency, ω_p'. A novel ^{3}He NMR calibration probe [57] provides a second calibration.

Information on the muon beam distribution is mainly accessed through two straw tracker stations [58] located inside the vacuum chamber 90 degrees apart in front of two calorimeter stations. While the trackers measure the decay positron trajectories, the information can be used to infer on the muon beam properties. Further information on the beam dynamics of the stored muons can be obtained from insertable fiber harp detectors located at 180 and 270 degrees from the injection point and the Injected Beam Monitoring System with one station each before and after the inflector magnet and an insertable third station in the storage region closely behind the injection point. The information obtained from these systems provides important input for determining several of the beam dynamics related corrections needed to obtain a_μ. A short summary of these corrections is provided in Sec. 3.3.

3 Run-1 data analysis summary

3.1 Analysis overview

Equation (2) is the basis for the determination of a_μ. It can be rewritten in terms of a ratio of two frequencies [11] and external, well-known constants as:

$$a_\mu = \frac{\omega_a}{\tilde{\omega}_p'(T_r)} \frac{\mu_p'(T_r)}{\mu_e(H)} \frac{\mu_e(H)}{\mu_e} \frac{m_\mu}{m_e} \frac{g_e}{2}. \tag{3}$$

Here, $\tilde{\omega}_p'(T_r)$ represents the magnetic field experienced by the stored muons in terms of the Larmor frequency of shielded protons in a spherical water sample at temperature $T_r = 34.7\,^\circ$C. The tilde indicates that this quantity is weighted by the actual muon distribution observed in the experiment. The ratio $\mu_e(H)/\mu_p'(T)$ of the magnetic moments of an electron bound in hydrogen to that of a proton shielded in a spherical water sample is measured to 10.5 ppb [59]. The bound-state QED corrections that determine the magnetic moment ratio of the electron bound in hydrogen versus a free electron, $\mu_e(H)/\mu_e$, are considered essentially exact [60], and the electron magnetic moment μ_e is known to 0.3 ppb [60]. The ratio of the mass of the muon and the mass of the electron, m_μ/m_e, is known to 22 ppb from the measurement of the hyperfine splitting of muonium [61] and bound-state QED [60]. Finally, the g factor of the electron, g_e is known to 0.13 ppt [3].

Equation (3) requires the measurement of the ratio $\omega_a/\tilde{\omega}_p'(T_r)$ to determine a_μ. Several terms enter into the determination of this ratio which can be conceptually written as [8]:

$$\frac{\omega_a}{\tilde{\omega}_p'(T_r)} \approx \frac{f_{\text{clock}} \cdot \omega_a^m \cdot (1 + C_e + C_p + C_{ml} + C_{pa})}{f_{\text{calib}} \cdot \langle \omega_p(x,y,\phi) \times M(x,y,\phi) \rangle \cdot (1 + B_k + B_q)}. \tag{4}$$

Here, f_{clock} represents a factor to compensate for the secret, slight detuning of the main experimental clock that was done to guarantee a fully blind analysis and ω_a^m is the measured anomalous spin precession frequency as outlined more in Sec. 3.2. The beam dynamics related corrections C_e, C_p, C_{ml}, and C_{pa} are further detailed in Sec. 3.3. The denominator comprises the factor f_{calib}, which accounts for the calibration of the trolley probes with the calibration probe. The term $\langle \omega_p(x,y,\phi) \times M(x,y,\phi) \rangle$ denotes the weighting of the field maps, $\omega_p(x,y,\phi)$, measured with the trolley and fixed probes with the beam distribution, $M(x,y,\phi)$, obtained from the straw detectors. Details about this analysis are provided in Sec. 3.4. The final corrections B_k and B_q stem from fast magnetic field transients from the kicker and quadrupole systems, respectively. More details will be given in Sec. 3.5 for B_q whereas B_k is described in detail in another contribution to this conference. Table 1 provides a summary for the Run-1 result for the corrections (C and B terms in Eq. (4)) and the uncertainties of the quantities in Eq. (4) and the external constants from Eq. (3).

3.2 Measuring ω_a^m

The measurement of ω_a is centered around the measured spin precession frequency, ω_a^m, as can be seen in the nominator of Eq. (4). The determination of ω_a^m succeeds through the measurement of the energy and time of the decay positrons in the 24 calorimeter stations. One of these calorimeter stations is shown in the left panel Fig. 3.

Due to the parity violating weak decay, high energy positrons are emitted preferentially along the direction of the muon spin, hence offering a means to observe the spin precession. For the analysis, the time distribution of decay positrons above an energy threshold of $E \sim 1.7$ GeV is histogrammed as shown in the right panel of Fig. 3.

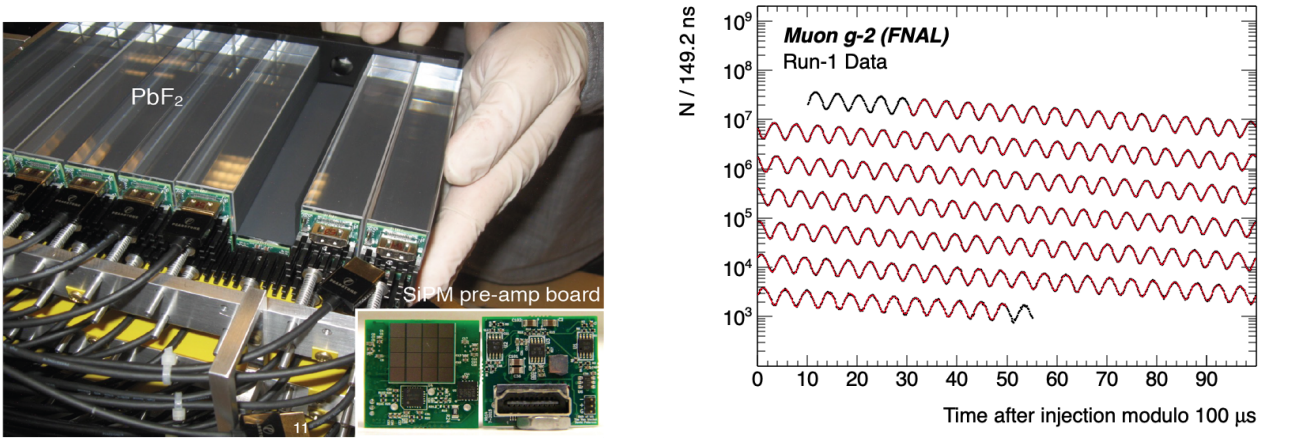

Figure 3. Left panel: Assembly of one of the 24 calorimeter stations each consisting of 54 PbF_2 crystals. The small insets show the silicon photomultipliers pre-amplifier board that are mounted on each crystal. Right panel: A typical wiggle plot - i.e., time distribution of detected positrons - for the Run-1 dataset.

Table 1. Summary of the Run-1 corrections and uncertainties for the quantities in Eq. (4) and external constants from Eq. (3).

Quantity	Correction (ppb)	Uncert. (ppb)
ω_a^m (stat.)	-	434
ω_a^m (syst.)	-	56
C_e	489	53
C_p	180	13
C_{ml}	-11	5
C_{pa}	-158	75
$f_{calib}\langle\omega_p(x,y,\phi)\times M(x,y,\phi)\rangle$	-	56
B_k	-27	37
B_q	-17	92
$\mu_p'(T_r)/\mu_e(H)$	-	10
m_μ/m_e	-	22
$g_e/2$	-	0
Totals	544	462

This so-called wiggle plot is the basis for the determination of ω_a^m and its main features can be described by the muon lifetime τ and the spin precession, ω_a^m, via $N(t) = N_0(t)e^{t/\tau}\left[1 - A\cos\omega_a^m t + \phi\right]$. The full analysis requires a more complicated fit function to account for various beam dynamics effects [10].

3.3 Beam dynamics corrections

A short summary of the four beam dynamics corrections, C_e, C_p, C_{ml}, and C_{pa} listed in the nominator of Eq. (4) is given here. Both the electric field correction C_e and the pitch correction C_p are related to the fact that Eq. (2) is only valid for ideal conditions of a horizontally circulating, magic-momentum muon in a vertical magnetic field. Given the momentum distribution and emittance of the muon beam, the full analysis must also take into account the additional terms in Eq. (1) as they do not fully vanish.

The muon momentum spread of $\Delta p/p \sim 0.15\,\%$ leads to not all muons being exactly on the magic momentum such that the $\vec{\beta}\times\vec{E}$ term has to be taken into account. The derivation of the correction is data driven and based on the equilibrium radius $\langle x_e^2\rangle$ of the muons. This quantity can be measured from the debunching of the initial, injected muon bunch. Two methods, one based on Fourier transform [62] and a direct fit of the debunching signal [43, 63] determined $\langle x_e^2\rangle$ with good agreement as shown in the left panel of Fig. 4. From the measured $\langle x_e^2\rangle$ distribution, an electric field correction $C_e = 489 \pm 53$ ppb was derived for the Run-1 result [9].

The pitch correction originate from the $\vec{\beta}\cdot\vec{B}$ term in Eq. (1) as the stored muons have a vertical angular distribution. Its determination is related to the vertical muon distribution [64, 65] which can be determined from the vertical decay position of electrons measured with the straw trackers, as shown in the middle panel of Fig. 4. The more involved determination includes acceptance corrections and other elements as detailed in [9] and led to a Run-1 correction of $C_p = 180 \pm 13$ ppb.

The number of stored muons during each injection cycle reduces not only through their decay into positrons but also due to some muons losing energy in elements like the beam shaping collimators or other materials and no longer being stored. These lost muons can carry different average phases from early to late in each muon fill. This would cause a change in the ω_a frequency over time. As these lost muons are no longer stored, they travel radially inward and being minimum ionizing particles, they leave small amounts of energy in neighboring calorimeters. Hence, a time coincidence of events in two or three neighboring calorimeters provides a way to measure the rate of lost muons and led to a correction of $C_{ml} = -11 \pm 5$ ppb.

The final correction is related to a movement of the muon beam during the storage time. The main origin for this beam movement in Run-1 was due to broken resistors in the electrostatic quadrupoles which led to a change in the quad high-voltage during muon storage and hence a change in their focusing strength. The determination of the so-called phase-acceptance correction included the use

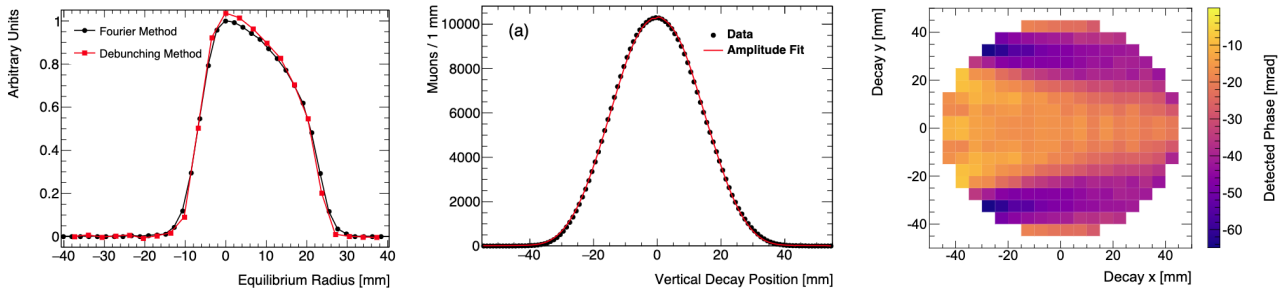

Figure 4. Left panel: The measured equilibrium radius determined with two methods. Middle panel: The vertical distribution of decay positron measured with the straw detectors. Right panel: The simulated phase map for decay positrons over the storage aperture.

of tracker data and simulated maps of the positron acceptance, asymmetry, and phase [9]. An example of the simulated phase map is shown in the right panel of Fig. 4. The correction applied in Run-1 was $C_{pa} = -158 \pm 75$, the second largest systematic uncertainty.

3.4 Measuring $\langle \omega_p(x,y,\phi) \times M(x,y,\phi) \rangle$

The measurement of the magnetic field in terms of the Larmor frequency of shielded protons weighted by the muon beam distribution, $\langle \omega_p(x,y,\phi) \times M(x,y,\phi) \rangle$, is one of the key ingredients in the denominator of Eq. (4). The term $\omega_p(x,y,\phi)$ is derived from the two main NMR systems in the experiment, namely the 378 fixed probes and the trolley system, the latter being shown in the left panel of Fig 5. Every 3 to 5 days, the muon beam injection is stopped and the trolley takes a full field map with about 9000 measurements for each of its 17 probes around the full 360° of the storage ring. The continuous measurements of the 378 fixed probes are synchronized to the detailed field maps taken by the trolley. Between trolley maps, the fixed probes then monitor the slow field drift. As they are arranged in groups of 4 and 6 probes in 72 azimuthal locations, they also provide some information about the higher order multipole drift. Both the detailed trolley measurements and the fixed probe information are analyzed using various methods including a Hilbert transform method [66] and are then combined in a complex analysis chain, to generate the frequency maps $\omega_p(x,y,\phi)$ [11].

The straw trackers provide the information needed to extract the muon distribution maps $M(x,y,\phi)$ over the course of the data taking. To extract the relevant information, the full analysis takes into account beam dynamics effects (such as beta functions) and detector acceptances of the trackers and the calorimeters.

3.5 Magnetic field transients

The pulsed injection systems used in the experiment, the fast magnetic kicker and the electric quadrupoles create magnetic transient fields that are too fast to be measurable with the main pulsed NMR probes employed. To investigate the magnetic field originating from the kicker, two Faraday magnetometers were built, one of them based on the magnetometer from E821 [67]. Details about magnetometer measurements are presented in a separate contribution to this conference.

In normal operating mode, the fixed probes are constantly taking measurements at ~1 Hz rate asynchronously with the beam injection. A special running mode was setup to trigger them relative to the beam injection with varying delay time. These special studies revealed a sizable change in the magnetic field which is now believed to be understood in terms of the mechanical vibrations of the quadrupole plates inducing magnetic fields. Since the NMR probes have a low bandwidth and are shielded by the vacuum chambers from high frequencies, a dedicated probe setup was developed to measure the effect in the storage region inside the quadrupoles. It was used to provide a detailed measurement of the change in the magnetic field before, during, and after muon injection. Fig 6 shows the sizable magnetic field change in the vicinity of one of the muon storage cycles. During the 700 µs of muon storage (gray band), the quadrupole induced field transient yields a change in the magnetic field of 100 – 200 ppb. A more detailed analysis [11] using measurements at various azimuthal and radial positions, averaging over all 16 different muon injection cycles, and folding the actual field change with the change in stored muons during the 700 μs yields a correction of $B_q = -17 \pm 92$, the single largest systematic uncertainty for the Run-1 result.

4 Summary and Outlook

The Run-1 result was based on about 6% of the total statistics that the experiment has collected and led to a confirmation of the BNL measurement, increasing the tension with the SM to 4.2 σ. Over the course of 2019 to 2023, a lot more data was collected. Fig. 7 shows the rate of data collection for all data taking periods (Run-1 through Run-6) in terms of the number of total BNL statistics. The technical design report's goal [7] of collecting 21 more statistics than BNL was reached in February 2023. Data analysis for the Run-2/3 datasets is close to final and on track to reduce the statistical uncertainty of the first result by a factor of 2 and bring the total systematic uncertainty to ~100 ppb. The unblinding of this ongoing analysis is expected in the late spring of 2023. The remaining datasets from Run-4, Run-5, and Run-6 will bring an-

Figure 5. Left panel: The in-vacuum field camera, the so-called trolley. Right panel: The azimuthally averaged magnetic field contours $\omega_p(x, y)$ overlaid with the azimuthally averaged muon distribution $M(x, y)$.

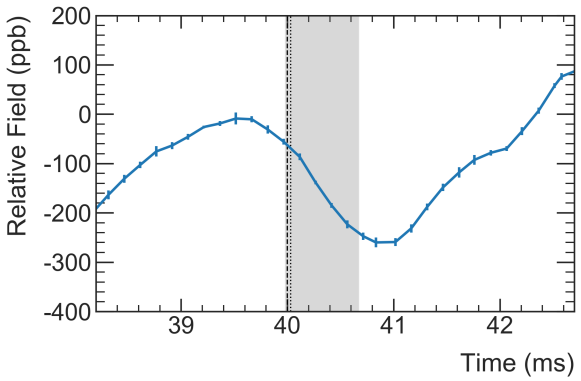

Figure 6. Measured change in field due to the quadrupole plate vibrations for one of the 16 muon injection cycles.

other factor of 2 for the total statistical uncertainty and some further reduction of the total systematic, leading to the anticipated overall factor of 4 improvement compared to BNL. After the first data taking period, a few key upgrades were performed that will help to reduce some of the systematic uncertainties compared to the Run-1 result. These upgrades include i) new qaudrupole resistors replacing the broken ones which will significantly reduce C_{pa}, ii) modifications of the kicker system to increase the voltage and center the beam radially, iii) thermal magnet insulation and better hall cooling to reduce the field drift, iv) improved quadrupole transient measurements significantly reducing the largest systematic uncertainty in Run-1, and v) a new RF system [68] which suppresses the coherent betatron oscillation amplitude and its associated systematic uncertainty. A final result for the Run-4/5/6 datasets is anticipated about 2-3 years from now.

5 Acknowledgments

This research was supported by the U.S. Department of Energy, Office of Science, High Energy Physics under contracts DE-AC02-06CH11357 (Argonne National Labo- ratory), and by Fermi National Accelerator Laboratory (Fermilab), a US DOE, HEP User Facility. Fermilab is managed by Fermi Research Alliance, LLC (FRA), acting under Contract No. DE-AC02-07CH11359.

References

[1] P.A.M. Dirac, Proc. R. Soc. A (London) **117**, 610 (1928)
[2] J.S. Schwinger, Phys. Rev. **73**, 416 (1948)
[3] X. Fan, T.G. Myers, B.A.D. Sukra, G. Gabrielse, Phys. Rev. Lett. **130**, 071801 (2023)
[4] R.H. Parker, C. Yu, W. Zhong, B. Estey, H. Müller, Science **360**, 191 (2018)
[5] L. Morel, Z. Yao, P. Cladé, S. Guellati-Khélifa, Nature **588**, 61 (2020)
[6] G.W. Bennett, B. Bousquet, H.N. Brown, G. Bunce, R.M. Carey, P. Cushman, G.T. Danby, P.T. Debevec, M. Deile, H. Deng et al. (Muon g-2), Phys. Rev. D **73**, 072003 (2006), hep-ex/0602035
[7] J. Grange, V. Guarino, P. Winter, K. Wood, H. Zhao, R.M. Carey, D. Gastler, E. Hazen, N. Kinnaird, J.P. Miller et al. (Muon g-2), arXiv:1501.06858 [physics.ins-det] (2015), 1501.06858
[8] B. Abi, T. Albahri, S. Al-Kilani, D. Allspach, L.P. Alonzi, A. Anastasi, A. Anisenkov, F. Azfar, K. Badgley, S. Baeßler et al. (Muon $g-2$), Phys. Rev. Lett **126**, 141801 (2021)
[9] T. Albahri, A. Anastasi, K. Badgley, S. Baeßler, I. Bailey, V.A. Baranov, E. Barlas-Yucel, T. Barrett, F. Bedeschi, M. Berz et al. (Muon $g-2$), Phys. Rev. Accel. Beams **24**, 044002 (2021)
[10] T. Albahri, A. Anastasi, A. Anisenkov, K. Badgley, S. Baeßler, I. Bailey, V.A. Baranov, E. Barlas-Yucel, T. Barrett, A. Basti et al. (Muon $g-2$), Phys. Rev. D **103**, 072002 (2021)
[11] T. Albahri, A. Anastasi, K. Badgley, S. Baeßler, I. Bailey, V.A. Baranov, E. Barlas-Yucel, T. Barrett, F. Bedeschi, M. Berz et al. (Muon $g-2$), Phys. Rev. A **103**, 042208 (2021)
[12] T. Aoyama, N. Asmussen, M. Benayoun, J. Bijnens, T. Blum, M. Bruno, I. Caprini, C.M. Carloni Calame, M. Cè, G. Colangelo et al., Phys. Rep. **887**, 1 (2020)
[13] T. Aoyama, M. Hayakawa, T. Kinoshita, M. Nio, Phys. Rev. Lett. **109**, 111808 (2012), 1205.5370

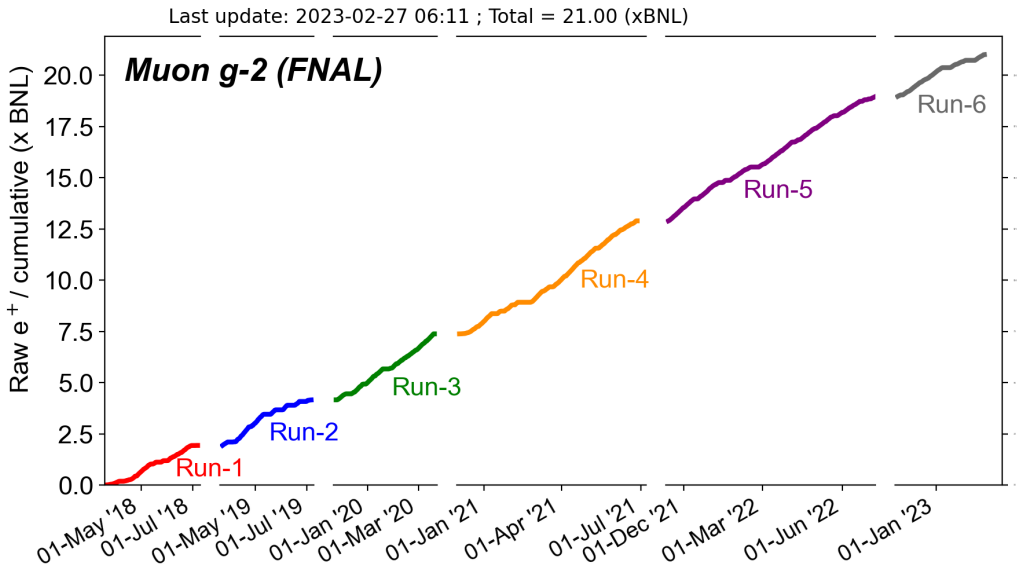

Figure 7. Raw collected statistics for all data taking periods. The technical design goal of 21× BNL statistics was reached in 02/2023.

[14] T. Aoyama, T. Kinoshita, M. Nio, Atoms **7**, 28 (2019)
[15] A. Czarnecki, W.J. Marciano, A. Vainshtein, Phys. Rev. **D67**, 073006 (2003), [Erratum: Phys. Rev. **D73**, 119901 (2006)], hep-ph/0212229
[16] C. Gnendiger, D. Stöckinger, H. Stöckinger-Kim, Phys. Rev. D **88**, 053005 (2013), 1306.5546
[17] M. Davier, A. Hoecker, B. Malaescu, Z. Zhang, Eur. Phys. J. **C77**, 827 (2017), 1706.09436
[18] A. Keshavarzi, D. Nomura, T. Teubner, Phys. Rev. **D97**, 114025 (2018), 1802.02995
[19] G. Colangelo, M. Hoferichter, P. Stoffer, J. High Energy Phys. **02**, 006 (2019), 1810.00007
[20] M. Hoferichter, B.L. Hoid, B. Kubis, J. High Energy Phys. **08**, 137 (2019), 1907.01556
[21] M. Davier, A. Hoecker, B. Malaescu, Z. Zhang, Eur. Phys. J. **C80**, 241 (2020), 1908.00921
[22] A. Keshavarzi, D. Nomura, T. Teubner, Phys. Rev. D **101**, 014029 (2020), 1911.00367
[23] A. Kurz, T. Liu, P. Marquard, M. Steinhauser, Phys. Lett. **B734**, 144 (2014), 1403.6400
[24] K. Melnikov, A. Vainshtein, Phys. Rev. D **70**, 113006 (2004), hep-ph/0312226
[25] P. Masjuan, P. Sánchez-Puertas, Phys. Rev. D **95**, 054026 (2017), 1701.05829
[26] G. Colangelo, M. Hoferichter, M. Procura, P. Stoffer, J. High Energy Phys. **04**, 161 (2017), 1702.07347
[27] M. Hoferichter, B.L. Hoid, B. Kubis, S. Leupold, S.P. Schneider, J. High Energy Phys. **10**, 141 (2018), 1808.04823
[28] A. Gérardin, H.B. Meyer, A. Nyffeler, Phys. Rev. D **100**, 034520 (2019), 1903.09471
[29] J. Bijnens, N. Hermansson-Truedsson, A. Rodríguez-Sánchez, Phys. Lett. B **798**, 134994 (2019), 1908.03331
[30] G. Colangelo, F. Hagelstein, M. Hoferichter, L. Laub, P. Stoffer, J. High Energy Phys. **03**, 101 (2020), 1910.13432
[31] T. Blum, N. Christ, M. Hayakawa, T. Izubuchi, L. Jin, C. Jung, C. Lehner, Phys. Rev. Lett. **124**, 132002 (2020), 1911.08123
[32] G. Colangelo, M. Hoferichter, A. Nyffeler, M. Passera, P. Stoffer, Phys. Lett. **B735**, 90 (2014), 1403.7512
[33] F.V. Ignatov, R.R. Akhmetshin, A.N. Amirkhanov, A.V. Anisenkov, V.M. Aulchenko, N.S. Bashtovoy, D.E. Berkaev, A.E. Bondar, A.V. Bragin, S.I. Eidelman et al. (CMD-3 Collaboration), *Measurement of the $e^+e^- \to \pi^+\pi^-$ cross section from threshold to 1.2 GeV with the CMD-3 detector* (2023), 2302.08834
[34] S. Borsanyi, Z. Fodor, J.N. Guenther, C. Hoelbling, S.D. Katz, L. Lellouch, T. Lippert, K. Miura, L. Parato, K.K. Szabo et al., Nature **593**, 51 (2021), 2002.12347
[35] C. Lehner, A.S. Meyer, Physical Review D **101**, 074515 (2020), 2003.04177
[36] G. Wang, T. Draper, K.F. Liu, Y.B. Yang, *Muon g-2 with overlap valence fermions* (2022), https://arxiv.org/abs/2204.01280
[37] C. Aubin, T. Blum, M. Golterman, S. Peris, Physical Review D **106**, 054503 (2022), 2204.12256
[38] M. Cè, A. Gérardin, G.v. Hippel, R.J. Hudspith, S. Kuberski, H.B. Meyer, K. Miura, D. Mohler, K. Ottnad, S. Paul et al., Physical Review D **106**, 114502 (2022), 2206.06582

[39] C. Alexandrou, S. Bacchio, P. Dimopoulos, J. Finkenrath, R. Frezzotti, G. Gagliardi, M. Garofalo, K. Hadjiyiannakou, B. Kostrzewa, K. Jansen et al., *Lattice calculation of the short and intermediate time-distance hadronic vacuum polarization contributions to the muon magnetic moment using twisted-mass fermions* (2022), https://arxiv.org/abs/2206.15084

[40] T. Blum, P.A. Boyle, M. Bruno, D. Giusti, V. Gülpers, R.C. Hill, T. Izubuchi, Y.C. Jang, L. Jin, C. Jung et al., *An update of Euclidean windows of the hadronic vacuum polarization* (2023), https://arxiv.org/abs/2301.08696

[41] A. Bazavov, C. Davies, C. DeTar, A.X. El-Khadra, E. Gámiz, S. Gottlieb, W.I. Jay, H. Jeong, A.S. Kronfeld, S. Lahert et al., *Light-quark connected intermediate-window contributions to the muon $g-2$ hadronic vacuum polarization from lattice QCD* (2023), https://arxiv.org/abs/2301.08274

[42] G. Charpak, F.J.M. Farley, R.L. Garwin, Phys. Lett. **1**, 16 (1962)

[43] J. Bailey, W. Bartl, G. von Bochmann, R.C.A. Brown, F.J.M. Farley et al., Nuovo Cim. A **9**, 369 (1972)

[44] J. Bailey et al. (CERN-Mainz-Daresbury), Nucl. Phys. B **150**, 1 (1979)

[45] A. Yamamoto et al., Nucl. Instrum. Meth. **A491**, 23 (2002)

[46] A. Schreckenberger, D. Allspach, D. Barak, J. Bohn, C. Bradford, D. Cauz, S. Chang, A. Chapelain, S. Chappa, S. Charity et al., Nuclear Instruments and Methods in Physics Research Section A: Accelerators, Spectrometers, Detectors and Associated Equipment **1011**, 165597 (2021)

[47] Y.K. Semertzidis, G. Bennett, E. Efstathiadis, F. Krienen, R. Larsen, Y.Y. Lee, W.M. Morse, Y. Orlov, C.S. Ozben, B.L. Roberts et al., Nucl. Instrum. Methods Phys. Res., Sect. A **503**, 458 (2003)

[48] M. Abe, S. Bae, G. Beer, G. Bunce, H. Choi, S. Choi, M. Chung, W. da Silva, S. Eidelman, M. Finger et al., Progress of Theoretical and Experimental Physics **2019** (2019)

[49] A.T. Fienberg, L.P. Alonzi, A. Anastasi, R. Bjorkquist, D. Cauz, R. Fatemi, C. Ferrari, A. Fioretti, A. Frankenthal, C. Gabbanini et al., Nucl. Instrum. Methods Phys. Res., Sect. A **783**, 12 (2015), 1412.5525

[50] J. Kaspar, A.T. Fienberg, D.W. Hertzog, M.A. Huehn, P. Kammel, K.S. Khaw, D.A. Peterson, M.W. Smith, T.D.V. Wechel, A. Chapelain et al., J. Instrum. **12**, P01009 (2017), 1611.03180

[51] K.S. Khaw, M. Bartolini, H. Binney, R. Bjorkquist, A. Chapelain, A. Driutti, C. Ferrari, A.T. Fienberg, A. Fioretti, C. Gabbanini et al. (Muon g-2), Nucl. Instrum. Methods Phys. Res., Sect. A **945**, 162558 (2019), 1905.04407

[52] A. Anastasi, A. Basti, F. Bedeschi, A. Boiano, E. Bottalico, G. Cantatore, D. Cauz, A.T. Chapelain, G. Corradi, S. Dabagov et al. (Muon g-2), J. Instrum. **14**, P11025 (2019), 1906.08432

[53] F. Bloch, W.W. Hansen, M. Packard, Phys. Rev. **69**, 127 (1946)

[54] E.M. Purcell, H.C. Torrey, R.V. Pound, Phys. Rev. **69**, 37 (1946)

[55] S. Corrodi, P.D. Lurgio, D. Flay, J. Grange, R. Hong, D. Kawall, M. Oberling, S. Ramachandran, P. Winter, J. Instrum. **15**, P11008 (2020)

[56] D. Flay, D. Kawall, T. Chupp, S. Corrodi, M. Farooq, M. Fertl, J. George, J. Grange, R. Hong, R. Osofsky et al., Journal of Instrumentation **16**, P12041 (2021), 2109.08992

[57] M. Farooq, T. Chupp, J. Grange, A. Tewsley-Booth, D. Flay, D. Kawall, N. Sachdeva, P. Winter, Phys. Rev. Lett. **124**, 223001 (2020)

[58] B. King, T. Albahri, S. Al-Kilani, D. Allspach, D. Beckner, A. Behnke, T. Bowcock, D. Boyden, R. Carey, J. Carroll et al., Journal of Instrumentation **17**, P02035 (2022)

[59] W.D. Phillips, W.E. Cooke, D. Kleppner, Metrologia **13**, 179 (1977)

[60] P.J. Mohr, D.B. Newell, B.N. Taylor, Rev. Mod. Phys. **88**, 035009 (2016), 1507.07956

[61] W. Liu, M.G. Boshier, S. Dhawan, O. van Dyck, P. Egan, X. Fei, M.G. Perdekamp, V.W. Hughes, M. Janousch, K. Jungmann et al., Phys. Rev. Lett. **82**, 711 (1999)

[62] Y. Orlov, C.S. Ozben, Y.K. Semertzidis, Nuclear Instruments and Methods in Physics Research Section A: Accelerators, Spectrometers, Detectors and Associated Equipment **482**, 767 (2002)

[63] F. Combley, E. Picasso, Physics Reports **14**, 1 (1974)

[64] F. Farley, Physics Letters B **42**, 66 (1972)

[65] F.J.M. Farley, E. Picasso, Adv. Ser. Direct. High Energy Phys. **7**, 479 (1990)

[66] R. Hong, S. Corrodi, S. Charity, S. Baessler, J. Bono, T. Chupp, M. Fertl, D. Flay, A. Garcia, J. George et al. (Muon $g-2$), Journal of Magnetic Resonance **329**, 107020 (2021), 2101.08412

[67] E. Efstathiadis, Y.Y. Lee, J.L. Mi, C. Pai, J.M. Paley, B.L. Roberts, R.T. Sanders, Y.K. Semertzidis, D.S. Warburton, Nucl. Instrum. Methods Phys. Res., Sect. A **496**, 8 (2003)

[68] O. Kim, M. Bhattacharya, S. Chang, J. Choi, J.D. Crnkovic, S. Ganguly, S. Hacĭömeroğlu, M. Kargiantoulakis, Y.I. Kim, S. Lee et al., New Journal of Physics **22**, 063002 (2020)